Research Article

Effects of Mn content on recrystallization resistance of AA6082 aluminum alloys during post-deformation annealing

Xiaoming Qian [1], Nick Parson [2], X.-Grant Chen [1, *]

[1] *Department of applied sciences, University of Quebec at Chicoutimi, Saguenay G7H 2B1, Canada*

[2] *Arvida Research and Development Centre, Rio Tinto Aluminum, Saguenay G7S 4K8, Canada*

* Corresponding author: Prof. X.-Grant Chen; Tel.: 1 418 545-5011, ext. 2603

E-mail address: xgrant_chen@uqac.ca (X.-Grant Chen).

The microstructural evolutions under as-homogenized and as-deformed conditions and after the post-deformation annealing of AA6082 aluminum alloys with different Mn contents (0.05–1 wt%) were studied by optical, scanning electron, and transmission electron microscopies. The results showed that the presence of a large amount of α-Al(Mn,Fe)Si dispersoids induced by Mn addition significantly improved the recrystallization resistance. In the base alloy free of Mn, static recrystallization occurred after 2 h of annealing, and grain growth commenced after 4 h of annealing, whereas in Mn-containing alloys, the recovered grain structure was well-retained after even 8 h of annealing. The alloy with 0.5% Mn exhibited the best recrystallization resistance, and a further increase of the Mn levels to 1% resulted in a gradual reduction of the recrystallization resistance, the reason for which was that recrystallization occurred only in the dispersoid-free zones (DFZs) and the increased DFZ fraction with Mn content led to an increase in the recrystallization fraction. The variation in the dispersoid number density and a coarsening of dispersoids during annealing have a limited influence on the static recrystallization in Mn-containing alloys.

Key words: AA6082 alloys; Mn effects; Recrystallization resistance; Dispersoid precipitation; Post-deformation annealing

1. Introduction

The traditional hardening mechanism of Al-Mg-Si 6xxx aluminum alloys is through the precipitation of fine nano-scale Mg_2Si precursor precipitates to attain superior mechanical properties at room temperature [1]. However, for a service temperature exceeding 200 °C, the mechanical properties deteriorate rapidly owing to the coarsening and dissolution of Mg_2Si precursors [2]. To develop alloys that can be applied at elevated temperatures, several studies have been conducted by the introduction of numerous thermally stable dispersoids in aluminum alloys [3-5]. For AA6082 aluminum alloys, one of the most common stable dispersoids encountered in the matrix is α-Al(Mn,Fe)Si, which is partially coherent and can be formed through decomposition of the supersaturated solid solution during homogenization [6, 7]. Li [8] reported that the precipitation of a large amount of α-Al(Mn,Fe)Si dispersoids can be promoted with the addition of Mn in 6082 alloys after a relatively low-temperature treatment at 400–450 °C, while the number density of dispersoids increases with an increase in the Mn levels. The strong effect of Mn addition on the precipitation of α-Al(Mn,Fe)Si dispersoids during high-temperature homogenization (550–580 °C) in 6082-based alloys was also reported by Liu [9, 10].

After casting and homogenization, 6xxx aluminum alloys are usually subjected to a thermomechanical process, such as rolling or extrusion to achieve a desirable shape. The deformed structures are usually associated with a high level of internal stress and a high density of the substructures. To achieve appropriate and stable mechanical and materials properties, a post-deformation heat treatment (annealing or solution treatment) is applied [11]. Statistic recovery (SRV) and statistic recrystallization (SRX) can occur during the post-deformation annealing. SRV is associated with a change in the density and distribution of line defects, whereas SRX involves the nucleation and growth of new grains as well as grain boundary migration [12]. The control of SRX plays an important role in wrought aluminum alloys. It has been reported that the occurrence of SRX negatively influences the corrosion resistance in 2xxx alloys [13, 14]. In 5xxx alloys, the work hardening effect can be kept only if the non-recrystallized structure can be maintained [15, 16]. In 7xxx alloys, a recrystallized structure can cause an increasing risk of weld cracking, a decreased fracture toughness, and a detrimental effect on the corrosion resistance [17-19].

The pre-existing thermally stable dispersoids in the aluminum matrix can significantly control grain growth and retard recrystallization owing to their pinning effect on grain boundary migration [20]. The size, number density, and distribution of the dispersoids have a

significant influence on the recrystallization resistance [21-25]. It has been well recognized that the presence of a number of fine Al_3Zr dispersoids can significantly increase the recrystallization resistance during post-deformation annealing in 7xxx alloys [21, 22]. Li et al. [23] studied the effects of Er and Zr on recrystallization in pure aluminum and found that Al3(Er,Zr) dispersoids can be formed during heat treatment at 400 °C for 48 h, resulting in a remarkable enhancement of the recrystallization resistance during annealing at 350–525 °C. Birol[24] reported that a superior recrystallization resistance of 6082 alloy can be obtained through a large population of Cr-rich Al(Cr,Mn,Fe)Si and $(Al,Si)_3Zr$ dispersoids. However, the individual addition of Mn or Zr fails to offer any improvement in the recrystallization resistance in 6082 tube extrusions. Tsivoulas et al. [25] investigated the effects of Mn and Zr additions on the recrystallization resistance in Al–Cu–Li 2198 sheets, and found that with a constant Zr level, the recrystallization resistance was diminished with the addition of Mn, and progressively worsened with a decrease in the amount of Zr as more Mn was added.

The above results on the dispersoid effect on the recrystallization resistance in aluminum alloys appear to be somewhat spread out and inconsistent owing to the complication of the recrystallization mechanism, which is attributed to the many factors involved, such as the alloying element and its content, deformation and annealing conditions. To date, no systemic studies on the effect of a Mn dispersoid-forming addition on the recrystallization resistance of 6082 alloys after a hot deformation can be found in the open literature. The evolution of the deformed microstructure during post-deformation annealing owing to the presence of numerous dispersoids, namely, the development of SRV and SRX, should be better understood.

In the present study, the effect of different Mn levels on the recrystallization resistance of AA6082 aluminum alloys was investigated. Direct chill cast billets were subjected to low-temperature homogenization at 450 °C for 6 h to promote the precipitation of Mn-containing dispersoids. The samples were then hot-deformed, followed by post-deformation annealing at 500 °C for up to 8 h. The microstructural evolutions under as-homogenized and as-deformed conditions and after post-deformation annealing were studied. Quantitative microstructural analyses were conducted on the dispersoid precipitation, SRV, and SRX to better understand the effects of dispersoids on the recrystallization resistance.

2. Experimental

Four 6082 direct chill (DC) cast alloys with Mn levels of 0.05%–1.0% were prepared for the investigation. The chemical compositions are shown in Table 1. The samples were taken

from DC cast billets with a diameter of 101 mm. To produce numerous dispersoids in the aluminum matrix, DC cast billets were heat-treated at 450 °C for 6 h, followed by water quenching at room temperature, prior to hot deformation.

After heat treatment, specimens with diameter 10 mm and length 15 mm were machined for compression tests, which were conducted in a Gleeble 3800 thermomechanical testing unit. The compression tests were carried out at 400 °C with a strain rate of 0.1 s-1 and a total true strain of 0.75. The specimens were heated with a heating rate of 2 °C/s to 400 °C, and then held for 180 s until the compression starts. After hot deformation, a post-deformation annealing was conducted at 500 °C for 2, 4, and 8 h to study the recrystallization behavior.

To reveal the details of the microstructure, an optical microscope (Nikon, Eclipse ME600) and a scanning electron microscope (SEM, JEOL-6480LV) were used to examine the microstructure of polished samples, which were etched with a 0.5% HF solution for 40 s. All deformed samples were sectioned parallel to the compression axis along the centerline and prepared using the standard metallographic procedure. An electron back-scattered diffraction (EBSD) analysis under SEM was applied to examine the grain structure after hot deformation and post-deformation annealing. The step size of the EBSD analysis was set to 0.5 μm. All Euler orientation maps were used in the EBSD image analysis, and boundary misorientation angles of 2–5°, 6–15°, and greater than 15° were used to distinguish the subgrain and grain structure. To avoid the noises caused by the sample surface preparation, misorientation angles of below 2° were not considered in the orientation maps. A transmission electron microscope (TEM, JEM−2100) operating at 200 kV was used to observe the details of the Mn-containing dispersoids. Twin-jet polishing with 30% nitric acid and a 70% methanol solution at 15 V and -20 °C was employed to prepare the TEM thin foils.

3. Results

3.1. Microstructure after homogenization

Fig. 1 shows typical microstructures of 0.5Mn and 1Mn alloys as example. As indicated, the microstructures were composed of the aluminum matrix, Fe-rich intermetallics (see the inset images) along the boundaries of dendrites and grains, and primary Mg_2Si (black color in the inset images) often located together with the Fe-rich intermetallics. In the base alloy with a trace of Mn, no precipitation occurred in the aluminum matrix after heat treatment. In three alloys containing Mn, numerous precipitates were observed in the aluminum matrix and were identified as α-Al(MnFe)Si dispersoids in our previous study [6]. In the 0.5Mn alloy, the

dispersoids are distributed uniformly and only very narrow dispersoid-free zones (DFZs) are observed in the interdendritic regions (Fig. 1a). However, with an increase in the Mn levels, the DFZs become enlarged and more recognizable. The 1Mn alloy possesses the highest amount of DFZs (Fig. 1b).

3.2. Microstructure after hot deformation

Samples after heat treatment were compressed at 400 °C. Fig. 2 shows the microstructures after hot deformation of the four alloys. Elongated grains perpendicular to the compression direction were mainly observed in deformed structures. The intermetallics were fragmented along the boundaries of dendrites and grains. In the base alloy, there are only a few separate particles of Mg_2Si in the aluminum matrix but no dispersoids. In the three alloys containing Mn, fine and dense dispersoids were observed in the aluminum matrix. DFZs are also elongated along the compression direction and are more obvious in the 0.75Mn and 1Mn alloys. An image analysis to quantify the dispersoid number density was conducted based on a series of SEM images (not shown here, see the example in Fig. 9). The area fraction of DFZs was measured based on a series of optical images. Fig. 3 shows the number density of dispersoids and the DFZ area fraction in the three Mn-containing alloys. The number density of the dispersoids increased with an increase in the Mn amount from 8.6 μm^{-2} in the 0.5Mn alloy to 10.2 and 15.3 μm^{-2} in the 0.75Mn and 1Mn alloys, respectively. For the DFZ area fraction, the 0.5Mn alloy is as low as 2.7%, whereas it increases significantly to 6.8% and 16.7% in the 0.75Mn and 1Mn alloys, respectively. The sizes of the dispersoids (the mean equivalent diameter) remained nearly unchanged (~75 nm) in the three Mn-containing alloys.

The grain structures were investigated using the EBSD technique. Fig. 4 shows all Euler orientation maps of the four experimental alloys after hot deformation. In addition to the elongated grains, numerous low- and medium-angle boundaries were observed, indicating the presence of high densities of dislocations and subgrains. The deformed microstructures of all four alloys typically showed a dynamically recovered structure without dynamic recrystallization [26]. Different densities of low-, medium-, and high-angle boundaries in the four alloys were observed, representing different DRV levels [27].

The misorientation angle boundaries were analyzed based on EBSD mapping, and the results are plotted in Fig. 5. The densities of a misorientation angle of greater than 15° in all four alloys are similar (within a range of 0.14–0.19 μm^{-1}) because the DRV during hot deformation has a limited influence on the high-angle grain boundaries. However, the density

of a misorientation angle of 2–15° (subgrain boundaries) increased from 0.35 μm^{-1} in the base alloy to 0.69 μm^{-1} in the 1Mn alloy. The increased density of a misorientation angle of 2–15o indicated a decline in the DRV levels with an increase in the Mn content and was believed to be related to the presence of a large amount of dispersoids. During hot deformation, the dispersoids acted as a strong barrier to the dislocation movement and subgrain migration [6, 28, 29]. With an increase in the dispersoid number density in the alloys, the dispersoids exerted a strong effect on the retardation of the DRV; thus, the DRV levels became lower with an increase in the Mn content (Fig. 5).

3.3. Microstructure evolution during post-deformation annealing

Post-deformation annealing was conducted at 500 °C for 2, 4, and 8 h. All Euler orientation maps of the annealed microstructures are shown in Fig. 6 as a function of the annealing time. In addition, specific data on the boundary densities with misorientation angles of 2–15° and >15° for the four alloys were analyzed, the results of which are plotted in Fig. 7.

For the base alloy after 2 h of annealing, the substructures became better organized (Fig. 6a) with less subgrains compared with the condition before annealing (Fig. 4a). Moreover, some newly formed grains were observed at near the original grain boundaries (as indicated by the arrows in Fig. 6a). These new grains were featured as being free of an internal substructure, indicating that partial statistic recrystallization (SRX) occurred during annealing [30, 31]. The density of the boundary between 2–15° was reduced to 0.23 μm^{-1} (Fig. 7a) compared with that before annealing (0.35 μm^{-1}, Fig. 5), whereas the density of a boundary greater than 15° increased slightly (from 0.14 to 0.16 μm^{-1}) owing to the occurrence of SRX, which is attributed to the formation of some new grains with high angle boundaries. With an increase in the annealing time to 4 and 8 h, abnormal grain growth occurred, whereby the grain size reached up to several hundred micrometers and few millimeters (Fig. 6b, c). Accordingly, the density of the boundary between 2–15° dropped to zero, indicating no substructure within the grains, whereas a boundary density of greater than 15° decreased to close to zero (Fig. 7a) owing to significant grain growth.

For the three Mn-containing alloys (0.5Mn, 0.75Mn and 1Mn alloys), elongated grains perpendicular to the compression direction were still observed and numerous substructures were always present after 2–8 h of annealing (Fig. 6d-l). In addition, no grain growth was observed after even 8 h of annealing, suggesting a much better recrystallization resistance than that of the base alloy. In the 0.5Mn alloy, the structure of the elongated grains was well retained

(Fig. 6a-c). However, the densities of the boundary at between 2–15° (0.33–0.38 μm^{-1}, Fig. 7b) were considerably lower than that of the condition before annealing (0.58 μm^{-1}, Fig. 5b), implying the occurrence of SRV during annealing. In addition, few newly equiaxed grains without an internal substructure can be observed at the original grain boundaries (as indicated by the arrows in Fig. 6e-f), suggesting the start of SRX to a limited extent. These recrystallized grains were much smaller compared with those in the base alloy after 2 h of annealing. The SRX resulted in only a small increase in the densities of the boundary at greater than 15° (0.19–0.20 μm^{-1}, Fig. 7b) compared with the condition before annealing (0.18 μm^{-1}, Fig. 5). A small number of recrystallized grains became recognizable, but remained at a low level in the 0.75Mn alloy (see the arrows in Fig. 6 g-i). With a further increase in Mn to 1%, a larger number of recrystallized grains appeared (see the arrows in Fig. 6 j-l) compared to the 0.75Mn alloy. These newly formed recrystallized grains brought about a corresponding increase in the boundary density of the misorientation angles over 15° (0.21–0.23 μm^{-1} in Fig. 7c and 0.30–0.32 μm^{-1} in Fig. 7d). Meanwhile, the densities of the boundary between 2–15° also increased with the Mn amount (Fig. 7c, d) owing to the increasing dispersoids number density, which led to a stronger retardation effect on the SRV.

Regarding the three Mn dispersoid-forming alloys, it was also found that the boundary structures did not exhibit an obvious change along with the annealing time (Fig. 6d-l), which was also reflected by the stability of the boundary densities along with the annealing time (Fig. 7b, c and d).

A quantitative image analysis was conducted on the recrystallized grain size and fraction for 0.5Mn, 0.75Mn and 1Mn alloys, the results of which are shown in Fig. 8. Both the size and volume fraction of the recrystallized grains increased with an increase in the Mn addition but remained nearly unchanged with the annealing time. For instance, after 4 h of annealing, the recrystallized grain size increased from 3.8 μm in the 0.5Mn alloy to 4.4 and 6.5 μm in the 0.75Mn and 1Mn alloys, respectively, whereas the volume fraction moderately increased from 2.1% in the 0.5Mn alloy to 5.2% in the 0.75Mn alloy and considerably to 14.7% in the 1Mn alloy. It should be noted that, although SRX occurred in the three Mn-containing alloys, the proportion of recrystallized grains is at a low level and the deformed microstructure after post-deformation annealing mostly maintains a recovered grain structure.

The evolution of the dispersoids in the 1Mn alloy during annealing is shown in Fig. 9. During annealing, a gradual coarsening and dissolution of the dispersoids took place, as implied by the smaller population and larger sizes of the dispersoids with an increase in the annealing time. The α-Al(MnFe)Si dispersoids are thermally stable within a temperature range

of 300–350 °C, and above these temperatures they become less stable [3,5]. The results obtained here confirm that the dispersoids during annealing at 500 °C were no longer stable. The changes in the number density of the dispersoids during annealing are shown in Fig. 10. The decrease in the number density of dispersoids with the annealing time occurred in all three alloys. However, the decline in the number density was mostly significant in the 1Mn alloy, and became less distinct in the alloy with a lower Mn content.

The DFZ area fraction in the 0.5Mn, 0.75Mn and 1Mn alloys during annealing was also measured. The results revealed that the DFZ area fraction after annealing in the three alloys remained nearly unchanged when compared with that before annealing (Fig. 3), suggesting that a coarsening and dissolution of dispersoids occurred only in the dispersoid zone and that the DFZs maintained their initial states.

4. Discussion

The effects of Mn and its dispersoid distribution on the recrystallization resistance of 6082 aluminum alloys were studied. A large amount of dispersoids were introduced through the addition of Mn and a low-temperature homogenization treatment. The presence of numerous dispersoids significantly improved the recrystallization resistance and avoided the severe grain growth during the post-deformation annealing compared with the base alloy. For the three Mn-containing alloys, the recrystallization resistance slightly decreased with an increase in the Mn addition.

In industrial practice, an excellent recrystallization resistance is desirable because a poor recrystallization resistance may cause or a recrystallized structure or a coarse grain structure during post-deformation heat treatment. In the current study, when the dispersoids were absent in the base alloy, 2 h of annealing at 500 °C resulted in the occurrence of SRX, whereas after 4 h of annealing, abnormal grain growth was observed, resulting in an extremely coarse grain structure (Fig. 6b and c). After the introduction of dispersoids in 0.5Mn, 0.75Mn and 1Mn alloys, the deformed microstructure was stabilized and the recovered grain structure was retained (Fig. 6d-l), showing an excellent recrystallization resistance under high-temperature annealing treatment.

Regarding the three dispersoid-containing alloys, the number density of the dispersoids increased with an increase in the Mn content after homogenization (Fig. 3). This increase in the number density leads to an increase in the substructure density after hot deformation (Fig. 4 and 5). In theory, a high number density of dispersoids can contribute to a better

recrystallization resistance during annealing owing to the strong pining ability on the grain boundary migration and the grain rotation [24, 32]. However, a contrary result in the present study was observed: The 0.5Mn alloy exhibited the best recrystallization resistance with the lowest SRX fraction, whereas the 0.75Mn alloy possessed a higher SRX fraction and the 1Mn alloy had even the highest (Fig. 6 and 8b).

The decreased recrystallization resistance with an increase in the Mn content was believed to be related to the DFZs. Fig. 11 shows a bright-field TEM image of the recrystallized grains in the 1Mn alloy after 8 h of annealing. Newly formed and recrystallized grains, featured as being free of internal substructures, can be clearly observed in the interdendrite region where large intermetallic particles are present. The location of these recrystallized grains was actually in the DFZ where nearly no dispersoids existed. However, in the neighbor regions, a large amount of dispersoids remained, representing a high density of substructures in the non-recrystallized grains. This result implies that during annealing, the newly recrystallized grains preferred to nucleate and grow at the DFZ where the pinning effect of dislocations is the weakest [33]. In addition, with the increase of the Mn content from 0.5 to 1 wt.%, the amount of intermetallic particles (Fe-rich intermetallic and primary Mg_2Si) moderately increased [8] and those particles were primarily located in DFZ zones. The higher amount of large intermetallic particles in the higher Mn-containing alloys can also favor the recrystallization in the DFZ zones by the particle-stimulated nucleation mechanism in some extent [34]. Once the recrystallized grains encountered the dispersoid zone, the growth was arrested, and thus the growth of recrystallized grains was restricted in the DFZ.

Fig. 12 shows additional evidence that SRX took place in the DFZs. Comparing an enlarged EBSD map with the optical image, it can be seen that the recrystallized grain band is well matched with the DFZ shape and distribution in the matrix. Furthermore, the size of the recrystallized grains (approximately 7 μm, Fig. 12a) was very close to the PFZ width (Fig. 12b). In addition, the DFZ area fractions of individual alloys correspond well with the recrystallization fractions. As mentioned above, the DFZ area fraction increased from 2.7% in the 0.5Mn alloy to 6.8% and 16.7% in the 0.75Mn and 1Mn alloys, respectively (Fig. 3), whereas the recrystallization fraction increased from 2.1% in the 0.5Mn alloy to 5.2% and 14.7% in the 0.75Mn and 1Mn alloys (Fig. 8b), respectively.

Fig. 13 shows a schematic of how the recrystallization took place. After a hot deformation, numerous substructures were induced at both the dispersoids zones and DFZs (Fig. 13a). During post-deformation annealing, the high temperature provided a driving force for the motion of dislocations and subgrains. In the dispersoid zone, owing to the strong pinning effect

of the dispersoids on the dislocations and subgrain boundaries, only SRV was able to take place. However, in the DFZs, SRX can start through a diminishment or coalescence of dislocations into the subgrains owing to the absence of dispersoids and the weakest pinning effect (Fig. 13b). In addition, within the PFZs, the region surrounding the large intermetallic particles was highly strained during hot deformation, resulting in a higher density of dislocations and subgrains compared to the other regions. During annealing, the nucleation of new grains preferred to occur near the intermetallic particles where the driving force was higher, which is known as a particle-stimulated nucleation of recrystallization [2, 34, 35]. As a result, DFZs acted as the preferred regions where the SRX started and propagated (Fig. 13c).

The coarsening and dissolution of the dispersoids occurred during the post-deformation' annealing in all three Mn-containing alloys owing to the less thermal stability of dispersoids at 500 °C (Figs. 9 and 10). However, the above results indicate that the recrystallization resistance was mainly controlled by the DFZ fraction and less influenced by the number density and coarsening of the dispersoids. It was reported that even a low density of dispersoids of 0.003 μm^{-2} can have a significant influence on the recrystallization resistance in Al-Mg-Si alloys [33]. The dispersoid densities after 8 h of annealing at 500 °C still ranged from 3.2 to 5.5 μm^{-2} in the three Mn-containing alloys (Fig. 10), which is probably sufficient for inhibiting recrystallization. Therefore, the distribution of dispersoids associated with the DFZ is in fact the predominant factor controlling the recrystallization resistance during the post-deformation annealing.

It is worthwhile to note that for structural applications, the hot-deformed 6082 alloys after post-deformation annealing/solution usually undergo an artificial aging to precipitate the nanoscale β''/β'-Mg_2Si phases and to achieve the adequately high strengths. The presence of a large number of dispersoids induced by Mn addition can consume a part of Si solutes, which may disfavor β''/β' precipitation. On the other side, the pre-existing dispersoids formed during homogenization could provide favorable nucleation sites for subsequent β''/β' precipitation owing to the multiple benefits of the nucleation effects between the dispersoids and Mg_2Si [36]. In addition to enhanced recrystallization resistance, it would be expected that the presence of dispersoids further improves the mechanical properties of final products.

5. Conclusions

(1) Through the addition of Mn and a low-temperature homogenization treatment at 450 °C, numerous α-Al(Mn,Fe)Si dispersoids were generated in the aluminum matrix of AA6082 aluminum alloys.

(2) During post-deformation annealing at 500 °C, the base alloy free of Mn and dispersoids exhibited the worst recrystallization resistance. After 2 h of annealing, SRX occurred, whereas after 4 h of annealing, abnormal grain growth occurred.

(3) The presence of a large number of dispersoids greatly stabilized the deformed structure and thus significantly improved the recrystallization resistance. Even after 8 h at 500 °C annealing, the recovered grain structure was well-retained in all Mn-containing 6082 aluminum alloys.

(4) In the Mn-containing alloys, static recrystallization took place in the dispersoid free zones and the recrystallization resistance was mainly controlled by the DFZ fraction. The increased PFZ fraction with an increase in the Mn content led to an increase in the recrystallization fraction. Among the three Mn-containing alloys, the alloy with 0.5% Mn exhibited the best recrystallization resistance owing to the minimum DFZs. With a further increase in the Mn content to 0.75% and 1%, the recrystallization resistance moderately deteriorated owing to the increase in the DFZ fraction.

Acknowledgements

The authors would like to acknowledge the financial support of the Natural Sciences and Engineering Research Council of Canada (Grant No. CRDPJ 514651-17) and Rio Tinto Aluminum through the Research Chair in the Metallurgy of Aluminum Transformation at University of Quebec in Chicoutimi.

References

[1] A. Cuniberti, A. Tolley, M.V. Castro Riglos, R. Giovachini, Influence of natural aging on the precipitation hardening of an AlMgSi alloy, Mater. Sci. Eng. A, 527 (2010) 5307–5311

[2] M. Usta, M.E. Glicksman, R.N. Wright The effect of heat treatment on Mg_2Si coarsening in aluminum 6105 alloy. Metall. Mater. Trans. A. 35 (2004) 435-438

[3] K. Liu, X.-G. Chen, Development of Al–Mn–Mg 3004 alloy for applications at elevated temperature via dispersoid strengthening, Mater. Des., 84 (2015) 340–350.

[4] Z. Li, Z. Zhang, X.-G. Chen, Microstructure, elevated-temperature mechanical properties and creep resistance of dispersoid-strengthened Al-Mn-Mg 3xxx alloys with varying Mg and Si contents, Mater. Sci. Eng. A, 708 (2017) 383–394.

[5] K. Liu, H. Ma, X.-G. Chen, Enhanced elevated-temperature properties via Mo addition in Al-Mn-Mg 3004 alloy, J. Alloy Comp., 694 (2017) 354–365.

[6] X. Qian, N. Parson, X.-G. Chen, Effects of Mn addition and related Mn-containing dispersoids on the hot deformation behavior of 6082 aluminum alloys, Mate. Sci. Eng. A, 764 (2019) 138253.

[7] C. L. Liu, H. Azizi-alizamini, N. C. Parson, W. J. Poole, Q. Du, Microstructure evolution during homogenization of Al−Mg−Si−Mn−Fe alloys: Modelling and experimental results, Trans. Nonferrous Met. Soc. China 27 (2017) 747−753

[8] C. Li, K. Liu, X.-G. Chen: Improvement of elevated-temperature strength and recrystallization resistance via Mn-containing dispersoid strengthening in Al-Mg-Si 6082 alloys, J. Mater. Sci. Techno., 39 (2020) 135-143

[9] C. Liu, Microstructure evolution during homogenization and its effect on the high temperature deformation behaviour in AA6082 based alloys, PhD thesis, The University of British Columbia, 2017, pp.74−92

[10] C. Liu, Q. Du, N. Parson, W. Poole, The interaction between Mn and Fe on the precipitation of Mn/Fe dispersoids in Al-Mg-Si-Mn-Fe alloys, Scripta Mater. 152 (2018) 59–63.

[11] S. Lin, Z. Nie, H. Huang, B. Li, Annealing behavior of a modified 5083 aluminum alloy, Mater. Des. 31 (2010) 1607–1612

[12] H.J. McQueen, S. Spigarelli, M.E. Kassner, and E. Evagelista, Hot Deformation and Processing of Aluminum Alloys, CRC, Bradenton, FL, 2011, pp.383-403

[13] J. Corral, E.A. Trillo, Y. Li, L.E. Murr, Corrosion of friction-stir welded aluminum alloys 2024 and 2195, Journal of Mater. Sci. Let., 19 (2000) 2117–2122.

[14] I.N. Fridlyand, A.M. Drits, A.A. Yeliseyev, Lightweight and high-temperature alloys and the processing of them, Nauka, Moscow (1986) 126-130.

[15] Y.W. Riddle, T.h. Sanders, A study of coarsening, recrystallization, and morphology of microstructure in Al-Sc-(Zr)-(Mg) alloys, Metal. Mater. Trans. A, 35 (2004) 341-350.

[16] R.R. Sawtell, C.L. Jensen, Mechanical properties and microstructures of Al-Mg-Sc alloys, Metal. Trans. A, 21 (1990) 421-430.

[17] K.H. Chen, H.C. Fang, Z. Zhang, X. Chen, G. Liu, Effect of of Yb, Cr and Zr additions on recrystallization and corrosion resistance of Al–Zn–Mg–Cu alloys, Mater. Sci. Eng. A, 497 (2008) 426–431

[18] M. B. Kannan, V.S. Raja, Enhancing stress corrosion cracking resistance in Al–Zn-Mg-Cu-Zr alloy through inhibiting recrystallization, Eng. Fracture Mech. 77 (2010) 249–256

[19] F.-S. Lin, E. A. Starke, Jr., The effect of copper content and degree of recrystallization on

the fatigue resistance of 7xxx type aluminum alloys: I. low cycle corrosion fatigue, Mater. Sci. Eng. A, 39 (1979) 27-41

[20] Y. Birol, Impact of partial recrystallization on the performance of 6005A tube extrusions, Eng. Fail. Anal. 17 (2010) 1110–1116.

[21] Z. Guo, G. Zhao, X.-G. Chen, Effects of two-step homogenization on precipitation behavior of Al3Zr dispersoids and recrystallization resistance in 7150 aluminum alloy, Mater. Charact. 102 (2015) 122–130.

[22] Z. Guo, G. Zhao, X.-G. Chen, Effects of homogenization treatment on recrystallization behavior of 7150 aluminum sheet during post-rolling annealing, Mater. Charact. 114 (2016) 79–87

[23] H. Li, Z. Gao, H. Yin, H. Jiang, X. Sua and J. Bin, Effects of Er and Zr additions on precipitation and recrystallization of pure aluminum, Scripta Mater. 68 (2013) 59–62

[24] Y. Birol, Effect of Cr and Zr on the grain structure of extruded EN AW 6082 alloy, Met. Mater. Int., 20(4) (2014) 727-732

[25] D. Tsivoulas, P.B. Prangnell, The effect of Mn and Zr dispersoid-forming additions on recrystallization resistance in Al–Cu–Li AA2198 sheet, Acta Mater. 77 (2014) 1–16

[26] M. Shakiba, N. Parson, X.-G. Chen, Hot Deformation Behavior and Rate-controlling Mechanism in Dilute Al–Fe–Si Alloys with Minor Additions of Mn and Cu, Mater. Sci. Eng. A, 636 (2015) 572-581

[27] M. Shakiba, N. Parson, and X.-G. Chen, Effect of Iron and Silicon Content on the Hot Compressive Deformation Behavior of Dilute Al-Fe-Si Alloys, J. Mater. Eng. Perform, 24(1) (2015) 405

[28] C. Shi, W. Mao, X.-G. Chen, Evolution of activation energy during hot deformation of AA7150 aluminum alloy, Mater. Sci. Eng. A, 571 (2013) 83–91

[29] C. Shi, X.-G. Chen, Effect of vanadium on hot deformation and microstructural evolution of 7150 aluminum alloy, Mater. Sci. Eng. A, 613 (2014) 91–102

[30] O.V. Mishin, D. Juul Jensen, and N. Hansen, Evolution of Microstructure and Texture during Annealing of Aluminum AA1050 Cold Rolled to High and Ultrahigh Strains, Metall. Mater. Trans. A, 41 (2010) 2936-2948

[31] C. Schafer, V. Mohles, G. Gottstein, Modeling of non-isothermal annealing: Interaction of recrystallization, recovery, and precipitation, Acta Mater. 59 (2011) 6574–6587

[32] J. D. Robson and P. B. Prangnell, Dispersoid Precipitation and Process Modelling in Zirconium Containing Commercial Aluminium Alloys, Acta Mater. 49 (2001) 599–613

[33] R. Hu, T. Ogura, H. Tezuka, T. Sato and Q. Liu, Dispersoid formation and

recrystallization behavior in an Al-Mg-Si-Mn alloy, J. Mater. Sci. Technol., 26(3) (2010) 237-243.

[34]F.J. Humphreys, The nucleation of recrystallization at second phase particles in deformed aluminum, Acta Metall. 25 (1977) 1323–1344.

[35]D.P. Field, L. Behrens and J.M. Root, Identification of Particle Stimulated Nucleation during Recrystallization of AA 7050, CMC, 14(3) (2009) 171–183.

[36]L. Lodgaard, N. Ryum, Precipitation of dispersoids containing Mn and/or Cr in Al–Mg–Si alloys, Mater. Sci. Eng. A, 283 (2000) 144-152

Figure and table captions

Table 1 Chemical composition (wt.%) of the experimental alloys

Fig. 1. Optical micrographs of (a) 0.5Mn and (b) 1Mn alloys after 0.5% HF etching for 40 s. The inset images are SEM micrographs of an unetched surface.

Fig. 2 Microstructures after hot deformation: (a) the base, (b) 0.5Mn, (c) 0.75Mn and (d) 1Mn alloys and (e) an enlarged SEM image of 1Mn alloy.

Fig. 3 The number density of dispersoids and DFZ area fraction in the different alloys after hot deformation.

Fig. 4 All Euler orientation maps of four experimental alloys after hot deformation: (a) the base, (b) 0.5Mn, (c) 0.75Mn and (d) 1Mn alloys; the white lines indicate 2–5°, the green lines indicate 5–15°, and the black lines indicate >15°.

Fig. 5 Densities of the misorientation angle boundary of experimental alloys after hot deformation.

Fig. 6 All Euler orientation maps of the experimental alloys after different annealing times; the white lines indicate boundaries of 2–5°, light green lines indicate boundaries of 5–15°, and black lines show boundaries of >15°.

Fig. 7 Densities of the misorientation angle boundary of 2–5° and over 15° in (a) the base, (b) 0.5Mn, (c) 0.75Mn and (d) 1Mn alloys with different annealing times.

Fig. 8 (a) Recrystallization grain size and (b) volume fraction of experimental alloys at different annealing times.

Fig. 9 SEM microimages of the dispersoid evolution in the 1Mn alloy (a) before annealing and (b) after annealing at 500 °C for 2, (c) 4, and (d) 8 h. Bright field TEM images are inset in (a) and (c).

Fig. 10 Number density of dispersoids in 0.5Mn, 0.75Mn and 1Mn alloys at different annealing times.

Fig. 11 Bright field TEM image of recrystallized grains in the 1Mn alloy after 8 h of annealing.

Fig. 12 (a) EBSD orientation map and (b) optical image of the 1Mn alloy after 8 h of annealing.

Fig. 13 A schematic of the recrystallization mechanism: (a) after deformation and before annealing, (b) formation of subgrains during annealing, and (c) formation of recrystallized grains.

Table list:

Table 1 Chemical composition (wt.%) of the experimental alloys

Alloy	Mg	Si	Fe	Mn	Al
Base	0.79	1	0.18	**0.05**	Bal.
0.5Mn	0.83	1.01	0.22	**0.50**	Bal.
0.75Mn	0.84	1.02	0.23	**0.72**	Bal.
1Mn	0.81	1.02	0.24	**0.99**	Bal.

Figure list:

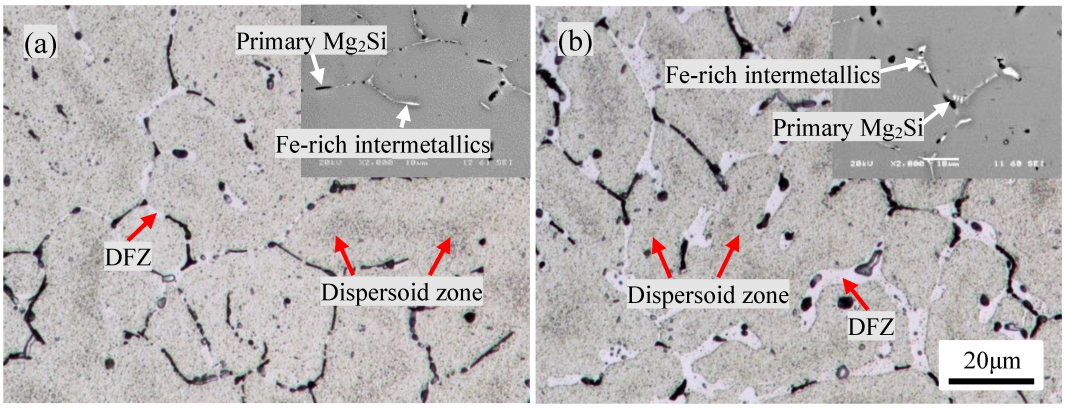

Fig. 1. Optical micrographs of (a) 0.5Mn and (b) 1Mn alloys after 0.5% HF etching for 40 s. The inset images are SEM micrographs of an unetched surface.

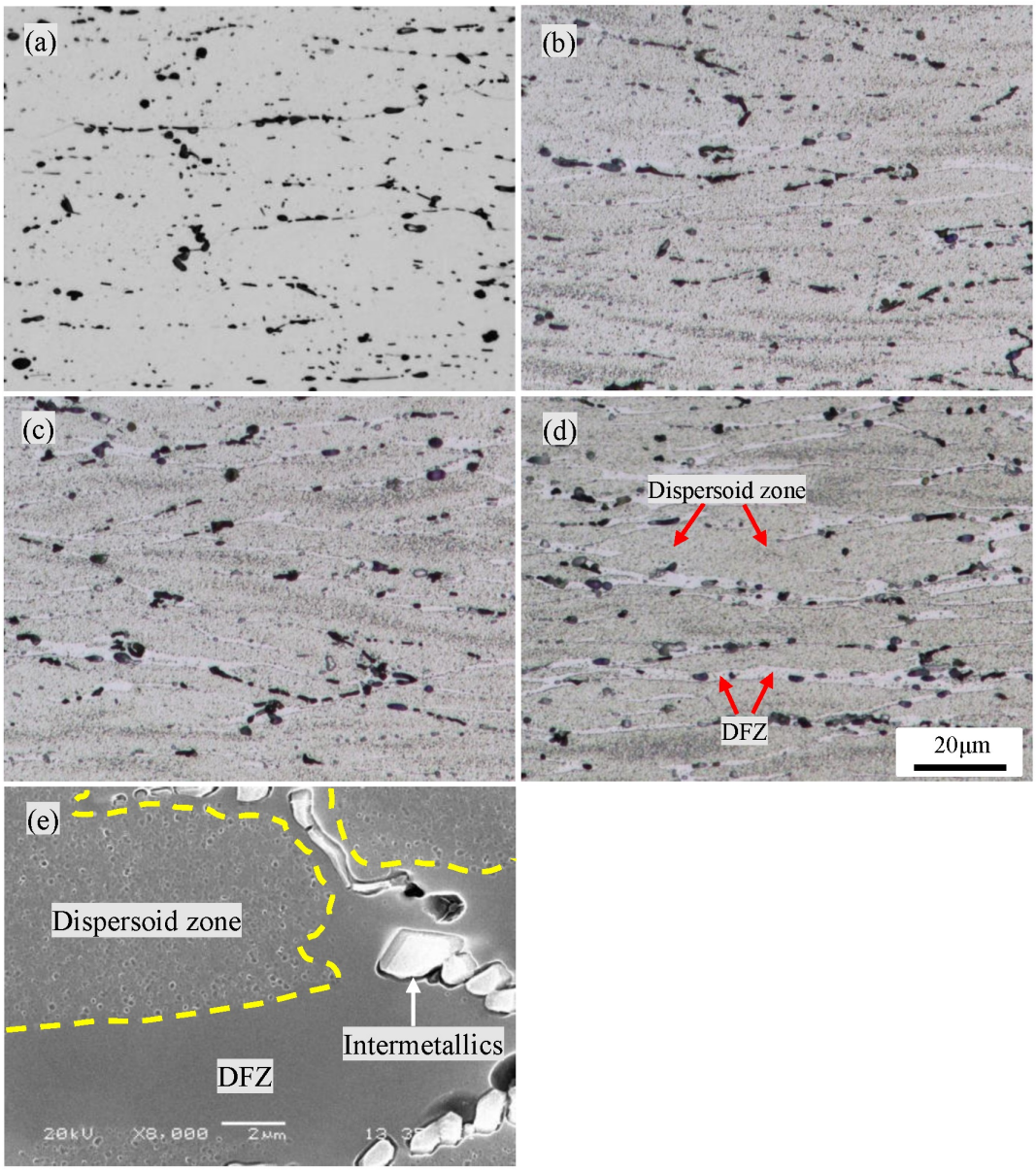

Fig. 2 Microstructures after hot deformation: (a) the base, (b) 0.5Mn, (c) 0.75Mn and (d) 1Mn alloys and (e) an enlarged SEM image of 1Mn alloy.

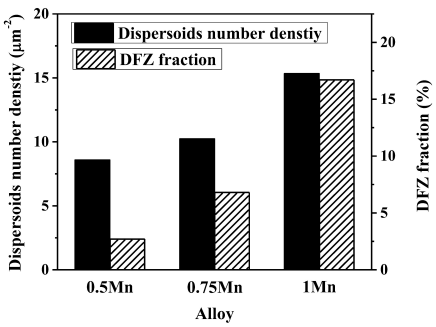

Fig. 3 The number density of dispersoids and DFZ area fraction in the different alloys after hot

deformation.

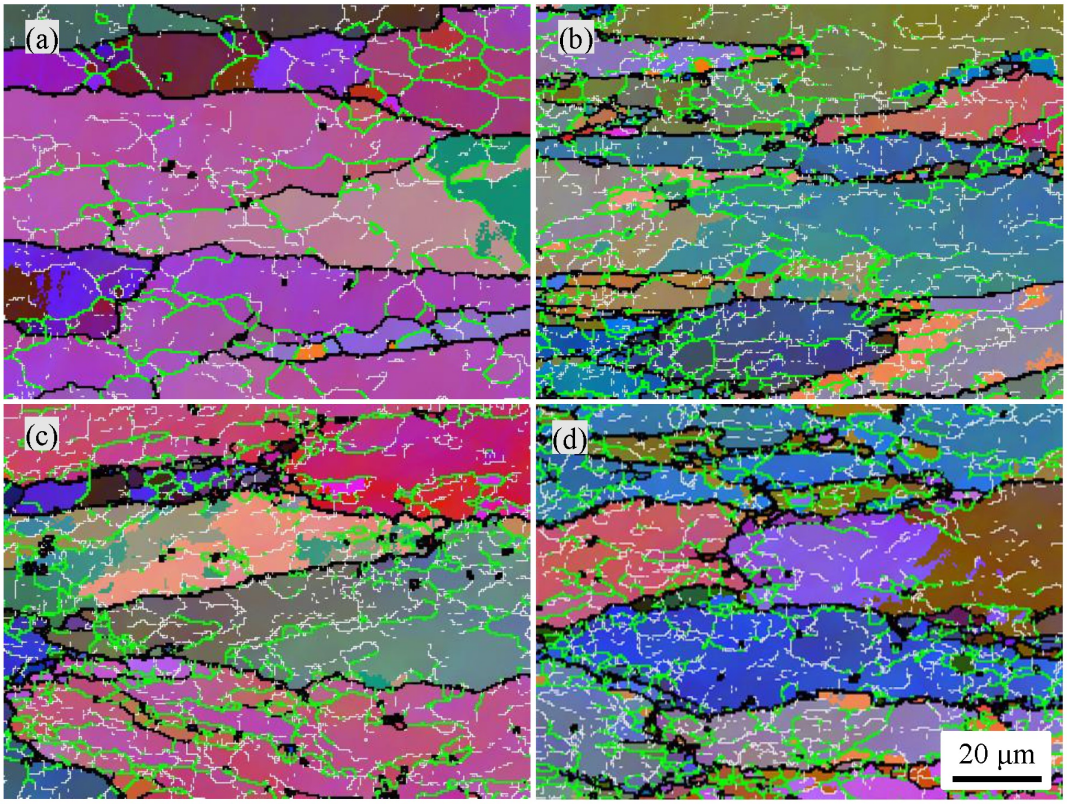

Fig. 4 All Euler orientation maps of four experimental alloys after hot deformation: (a) the base, (b) 0.5Mn, (c) 0.75Mn and (d) 1Mn alloys; the white lines indicate 2–5°, the green lines indicate 5–15°, and the black lines indicate >15°.

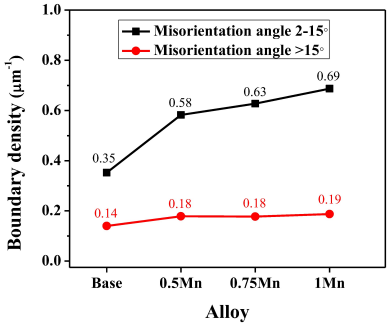

Fig. 5 Densities of the misorientation angle boundary of experimental alloys after hot deformation.

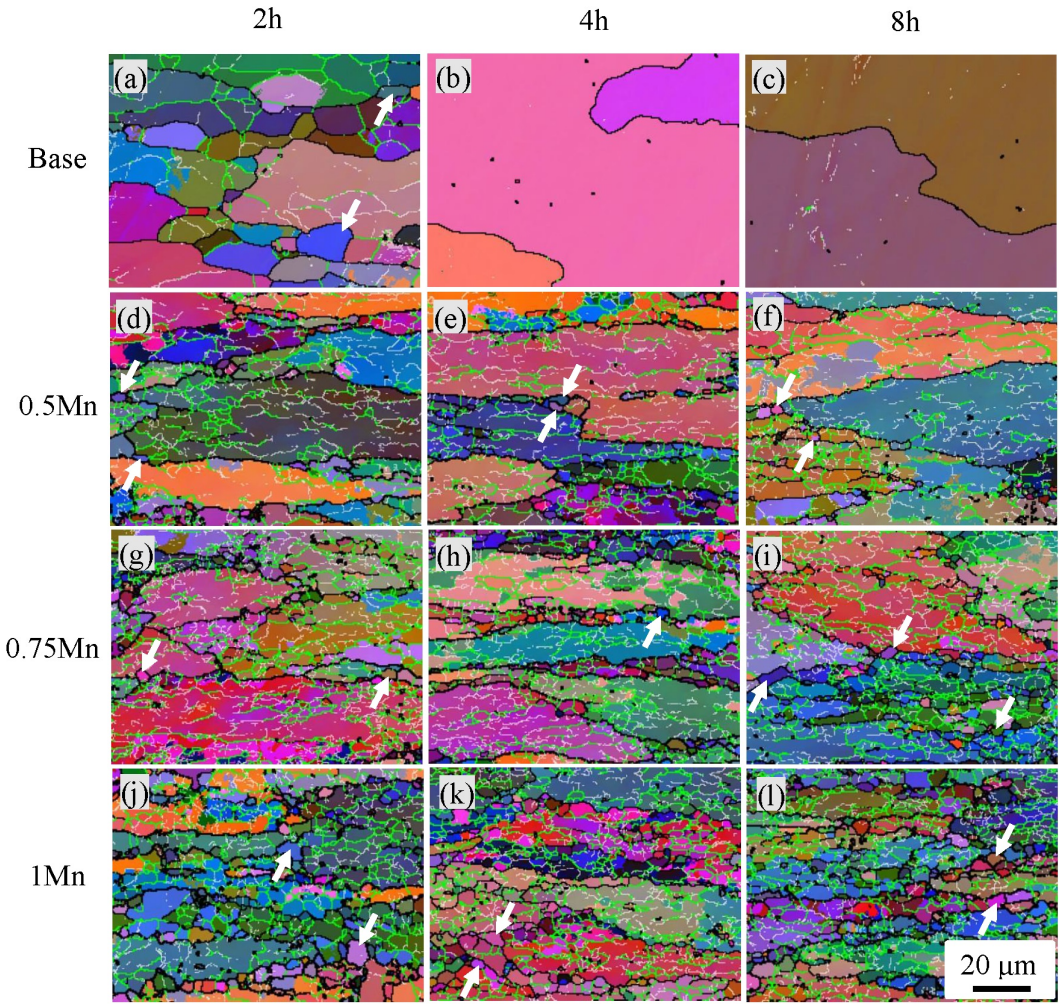

Fig. 6 All Euler orientation maps of the experimental alloys after different annealing times; the white lines indicate boundaries of 2–5°, light green lines indicate boundaries of 5–15°, and black lines show boundaries of >15°.

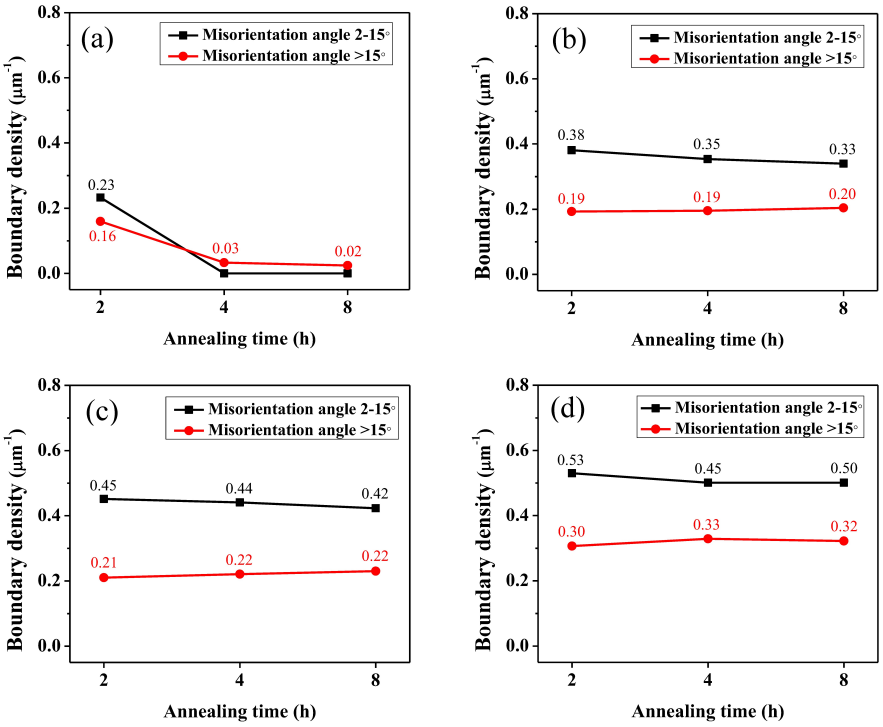

Fig. 7 Densities of the misorientation angle boundary of 2–5° and over 15° in (a) the base, (b) 0.5Mn, (c) 0.75Mn and (d) 1Mn alloys with different annealing times.

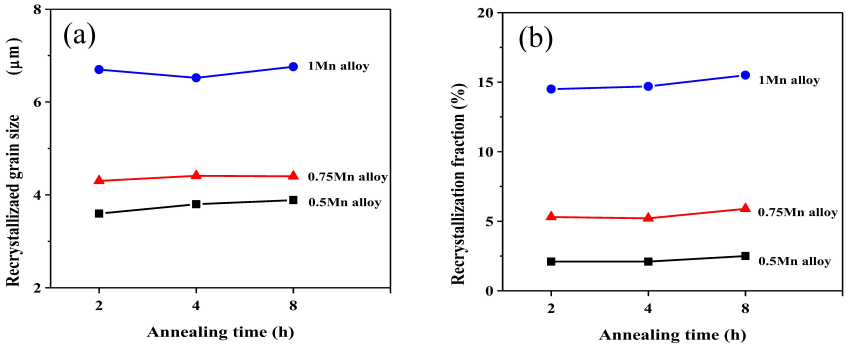

Fig. 8 (a) Recrystallization grain size and (b) volume fraction of experimental alloys at different annealing times.

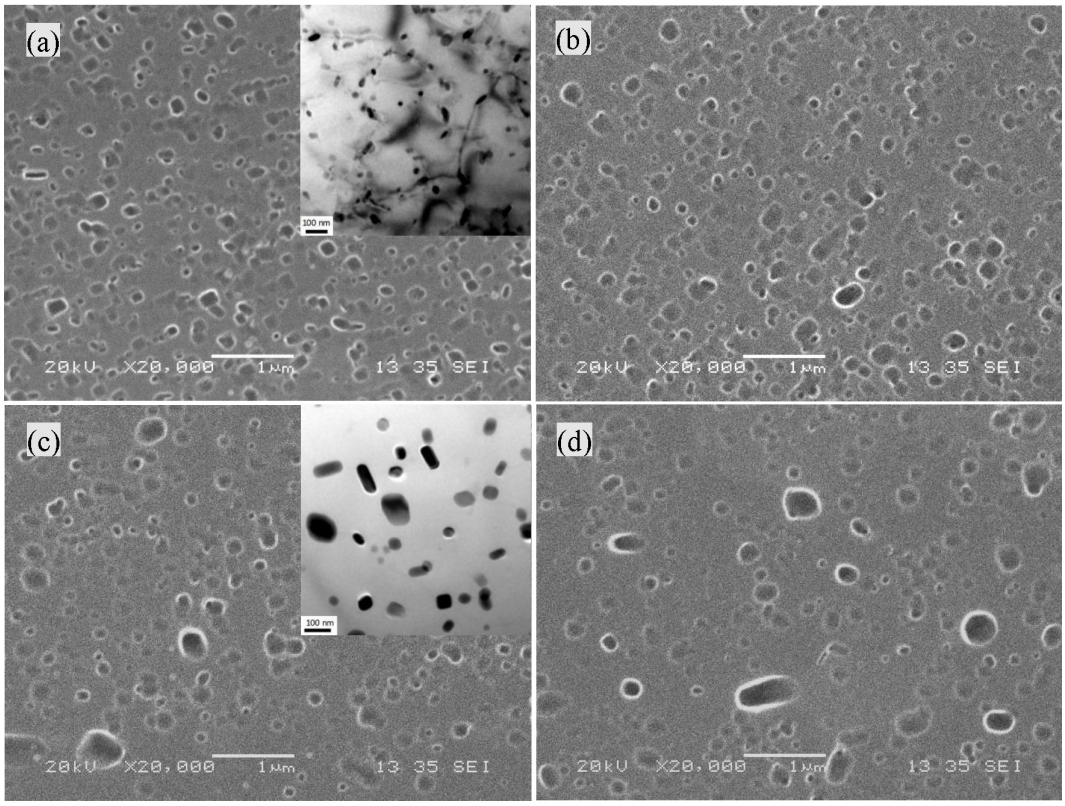

Fig. 9 SEM microimages of the dispersoid evolution in the 1Mn alloy (a) before annealing and (b) after annealing at 500 °C for 2, (c) 4, and (d) 8 h. Bright field TEM images are inset in (a) and (c).

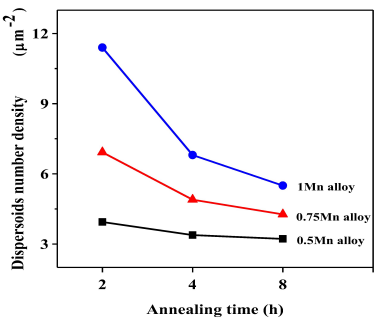

Fig. 10 Number density of dispersoids in 0.5Mn, 0.75Mn and 1Mn alloys at different annealing times.

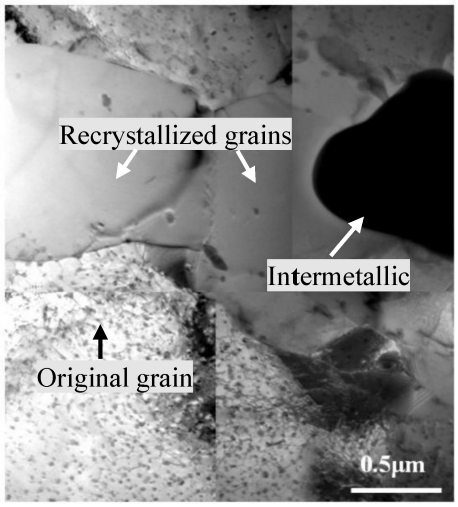

Fig. 11 Bright field TEM image of recrystallized grains in the 1Mn alloy after 8 h of annealing.

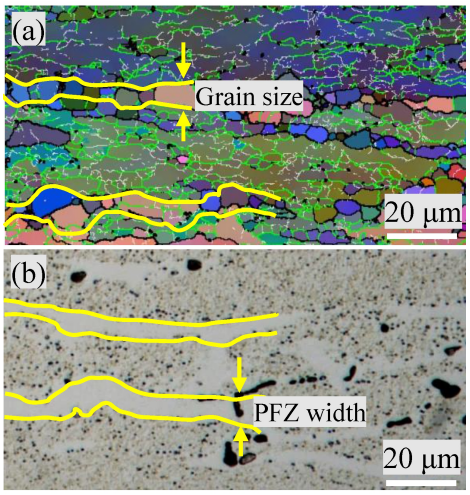

Fig. 12 (a) EBSD orientation map and (b) optical image of the 1Mn alloy after 8 h of annealing.

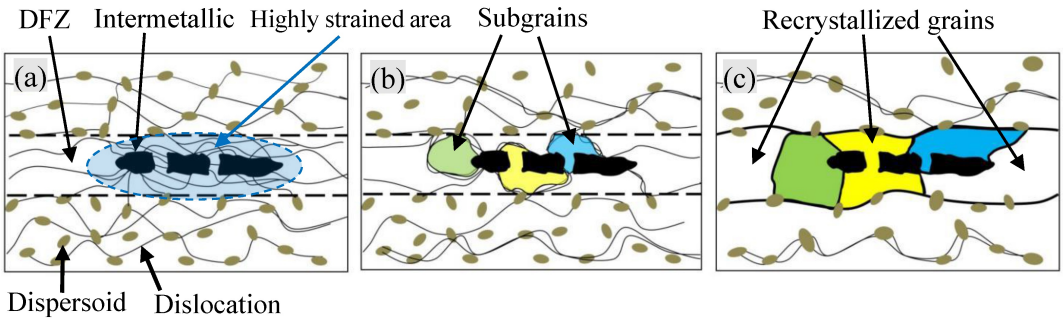

Fig. 13 A schematic of the recrystallization mechanism: (a) after deformation and before annealing, (b) formation of subgrains during annealing, and (c) formation of recrystallized grains.